Accepted Manuscript

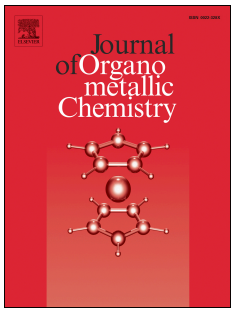

Synthesis and characterization of ferrocene-based Schiff base and ferrocenecarboxaldehyde oxime and their adsorptive removal of methyl blue from aqueous solution

Jamal Lasri, Abeer S. Elsherbiny, Naser Eltaher Eltayeb, Matti Haukka, Mohamed E. El-Hefnawy

PII: S0022-328X(18)30234-1

DOI: 10.1016/j.jorganchem.2018.04.004

Reference: JOM 20396

To appear in: *Journal of Organometallic Chemistry*

Received Date: 31 March 2018

Accepted Date: 4 April 2018

Please cite this article as: J. Lasri, A.S. Elsherbiny, N.E. Eltayeb, M. Haukka, M.E. El-Hefnawy, Synthesis and characterization of ferrocene-based Schiff base and ferrocenecarboxaldehyde oxime and their adsorptive removal of methyl blue from aqueous solution, *Journal of Organometallic Chemistry* (2018), doi: 10.1016/j.jorganchem.2018.04.004.

Synthesis and characterization of ferrocene-based Schiff base and ferrocenecarboxaldehyde oxime and their adsorptive removal of Methyl Blue from aqueous solution

Jamal Lasri[a,*], Abeer S. Elsherbiny[a,b], Naser Eltaher Eltayeb[a], Matti Haukka[c], Mohamed E. El-Hefnawy[a,b]

[a] *Department of Chemistry, Rabigh College of Science and Arts, P.O. Box 344, King Abdulaziz University, Jeddah, Saudi Arabia*

[b] *Department of Chemistry, Faculty of Science, Tanta University, Tanta 31527, Egypt*

[c] *University of Jyväskylä, Department of Chemistry, University of Jyväskylä, P.O. Box 35, FI-40014, Finland*

* Corresponding author.

E-mail address: jlasri@kau.edu.sa (J. Lasri).

ABSTRACT

The ferrocene-based Schiff base **3** was synthetized by reaction of ferrocenecarboxaldehyde **1** with 4-aminoantipyrine **2**. However, the reaction of **1** with hydroxylamine affords ferrocenecarboxaldehyde oxime **4**. Compounds **3** and **4** were fully characterized by IR, ^{1}H, ^{13}C and DEPT-135 NMR spectroscopy, elemental analyses and also by single crystal X-ray diffraction. Compounds **3** and **4** were used to remove anionic methyl blue dye from wastewater. The results established that both compounds have high adsorption capacity towards methyl blue. Langmuir adsorption capacity of compound **4** (464 mmol/g) is much higher than that of compound **3** (193 mmol/g) at 25°C. The kinetics data was fitted well pseudo-second-order model. Thermodynamic studies show that the adsorption of methyl blue onto compound **3** was endothermic, while its exothermic in case of adsorption onto compound **4**. The process was spontaneous for both compounds.

Keywords: Ferrocene-based Schiff base, Ferrocenecarboxaldehyde oxime; Single crystal X-ray diffraction; Adsorption; Methyl blue dye

1. Introduction

The extended use of synthetic dyes and the consequent ecological contamination due to release of wastewater polluted with dyestuffs become a critical issue nowadays [1]. Those dyes are non-biodegradable and display higher stability to light, heat, and oxidizing agents [2]. Methyl blue dye (MB) is used in different industrial applications such as textiles, packaging materials, paper products, paints, magnetic toners, color fiber, highlighters and inks [3,4,5]. Wastewater containing dyestuffs has been considered as a serious environment offender, because of its toxicity to biological systems and the damage on the public's health [6]. Hence, removal of hazardous dye (MB) is significant. Among recycling technologies and various water purification, adsorption is considered a promising method in treatment of water contaminated by dyes. Advantages of adsorption are relatively cheap operation, ease separation from filter, non-introduction of toxicities and highly selective for the chemical pollutant under consideration.

Currently, compounds containing ferrocene (Fc) moiety have been of considerable interest for their application in environmental pollution remediation of both organics and inorganics. Because ferrocene is electron rich and it can lose an electron to form Fc^+ [4,7], it can be regenerated by obtaining an electron which may allow it mitigate the repulsion in the adsorption process. Hence, these ferrocene-based compounds can provide enhanced affinity and adsorption capability toward pollutants [7].

On the other hand, oximes, HO–N=CRR', are valuable and simple reagents containing the O–N=C fragment, which can be added to nitrile ligands, to form a variety of nitrogen-containing compounds *e.g.* iminoacylated [8,9], amidines [10], carboxamides [11], phthalocyanines [12], or 1,3,5-triazapentadiene species [13].

This work attempts to assess the effects of ferrocene-based Schiff base **3** and ferrocenecarboxaldehyde oxime **4** with respect to the kinetics and adsorption isotherm

parameters of MB dye from aqueous solution as a model for wastewater remediation process.

2. Experimental Section

2.1. General methods

Reagents and solvents were obtained from Sigma-Aldrich. ^{1}H, ^{13}C and DEPT-135 NMR spectra (in $CDCl_3$) were measured on Bruker Avance III HD 600 MHz (Ascend^{TM} Magnet) spectrometer at ambient temperature. ^{1}H, ^{13}C and DEPT-135 chemical shifts (δ) are expressed in ppm relative to TMS. Infrared spectra (400-4000 cm^{-1}) were recorded on an Alpha Bruker FT-IR instrument in KBr pellets.

*2.2. Synthesis of ferrocene-based Schiff base **3** from ferrocenecarboxaldehyde **1** and 4-aminoantipyrine **2***

To a solution of ferrocenecarboxaldehyde **1** (2.33 g, 10.88 mmol) in methanol (10 mL) was added 4-aminoantipyrine **2** (2.21 g, 10.88 mmol) and the mixture was refluxed for 1 h. The precipitate formed was then filtered off and the filtrate was evaporated *in vacuo* to furnish the pure ferrocene-based Schiff base **3** in *ca.* 80% yield (Scheme 1).

*Trans-4-(ferrocenylideneamino)-1,5-dimethyl-2-phenyl-1H-pyrazol-3(2H)-one (**3**)* [14]
IR (cm^{-1}): 1642 (C=N), 1598 (C=C). ^{1}H NMR ($CDCl_3$), δ: 2.42 (s, 3H, CH_3C), 3.11 (s, 3H, CH_3N), 4.23 (s, 5H, CH_{Fc}), 4.42 (s, 2H, CH_{Fc}), 4.75 (s, 2H, CH_{Fc}), 7.32 (s, 1H, CH_{ar}), 7.47 (s, 4H, CH_{ar}), 9.52 (s, 1H, C(H)=N). ^{13}C NMR ($CDCl_3$), δ: 10.3 (CH$_3$C), 36.2 (CH$_3$N), 68.2 (CH$_{Fc}$), 69.4 (CH$_{Fc}$), 70.6 (CH$_{Fc}$), 82.3 (C_{Fc}), 120.1 (MeC=C), 124.0 (CH$_{ar}$), 126.6 (CH$_{ar}$), 129.1 (CH$_{ar}$), 135.0 (C_{ar}), 150.5 (MeC=C), 159.8 (C(N)=O), 161.2 (C(H)=N). Analysis calculated for $C_{22}H_{21}FeN_3O$: C 66.18, H 5.30, N 10.52%; found: C 66.11, H 5.39, N 10.61%.

*2.3. Synthesis of ferrocenecarboxaldehyde oxime **4** from ferrocenecarboxaldehyde **1** and hydroxylamine hydrochloride*

To a solution of hydroxylamine hydrochloride (0.83 g, 11.97 mmol) in methanol (10 mL) was added sodium carbonate (0.63 g, 5.98 mmol). The mixture was stirred for 5 min. Then, ferrocenecarboxaldehyde **1** (2.33 g, 10.88 mmol) was added and the reaction mixture was stirred at room temperature for 12 h. The precipitate formed was then filtered off and the filtrate was evaporated *in vacuo*. The product was washed with hexane (10 mL) to afford the pure ferrocenecarboxaldehyde oxime **4** in *ca*. 85% yield (Scheme 2).

*Ferrocenecarboxaldehyde oxime (**4**)* [15]
IR (cm^{-1}): 3195 (OH), 1630 (C=N). ^{1}H NMR ($CDCl_3$), δ: 4.25 (s, 5H, CH_{Fc}), 4.38 (s, 2H, CH_{Fc}), 4.57 (s, 2H, CH_{Fc}), 8.02 (s, 1H, C(*H*)=N). ^{13}C NMR ($CDCl_3$), δ: 67.6 (*C*H_{Fc}), 69.3 (*C*H_{Fc}), 70.1 (*C*H_{Fc}), 76.1 (*C*$_{Fc}$), 150.0 (*C*(H)=N). DEPT-135 NMR ($CDCl_3$), δ: 67.6 (*C*H_{Fc}), 69.3 (*C*H_{Fc}), 70.1 (*C*H_{Fc}), 150.0 (*C*(H)=N). Analysis calculated for $C_{11}H_{11}FeNO$: C 57.68, H 4.84, N 6.11%; found: C 57.60, H 4.89, N 6.19%.

2.4. Adsorption studies

Methyl blue dye (MB), (CI No. 42780) was purchased from Sigma-Aldrich and used as model of azo dye, its chemical structure was shown in Fig. 1. All adsorption experiments were done using doubly distilled water. A weighted 6 mg of **3** and/or **4** was added in a number of 100 mL conical flasks followed by adding 3mL of doubly distilled water and 3 mL of MB (2×10^{-4} M). The conicals were put in water shaker thermostat (Unitronic OR Selecta) at 25 ± 0.2 °C and 60 rpm. At predetermined time intervals, the **3** and/or **4** was removed from the solution and the concentration of nonadsorbed MB was determined by measuring the absorbance of the solution at λ_{max} = 585 nm using Perkin Elmer UV/Vis Spectrometer Lambda 35. The adsorption capacity q_e, was calculated by Eq. (1):

$$q_e = (C_o - C_e)V / m \qquad (1)$$

Where, C_o and C_e are the initial and equilibrium concentrations (mol L^{-1}) of MB, respectively, V is the volume (mL) of MB solution, and m is the mass (g) of adsorbent used.

The same experiment was done at 20, 30 and 40 ± 0.2 °C, respectively, to investigate the effect of temperature.

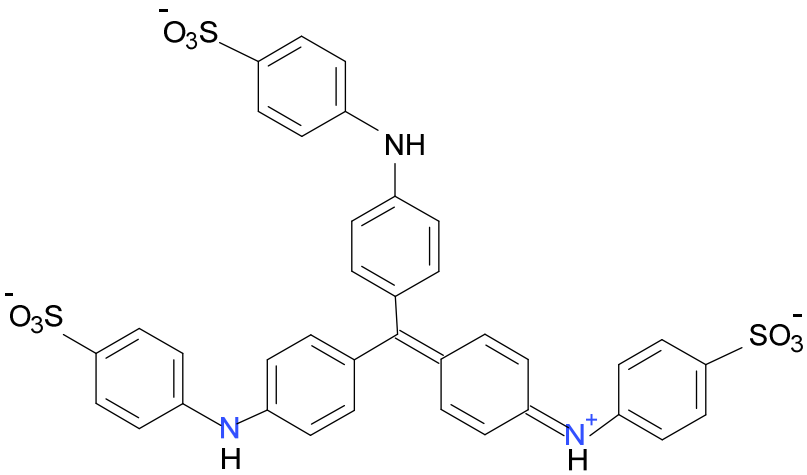

Fig. 1. Chemical structure of MB.

*2.5. Crystallography of ferrocene-based Schiff base **3** and ferrocenecarboxaldehyde oxime **4***

The crystals of **3** and **4** were obtained from methanol by slow evaporation. The crystals of **3** and **4** were measured at room temperature on a D8 QUEST Bruker Diffractometer using Mo Kα (λ = 0.71073) radiation. The *Apex3* [16] program package was used for cell refinements and data reductions. Multi-scan absorption correction (*SADABS*) [17] was applied to the intensities before structure solution. The structures were solved by intrinsic phasing method using the *SHELXT* [18] software. Structural refinement was carried out using *SHELXL-2017* [18]. The NOH group was disordered over two sites with occupancy ratio of 0.75/0.25. The N-O distances in the two disordered fragments were set to be similar. Furthermore, the oxygen atom O7B was restrained so that its U_{ij} components approximate to isotropic behavior. All H-atoms were positioned geometrically and

constrained to ride on their parent atoms, with C-H = 0.93 Å, O-H = 0.82 Å, and U_{iso} = 1.2-1.5·U_{eq} (parent atom). The crystallographic details are summarized in Table 1.

Table 1. Crystal Data of **3** and **4**.

	3	**4**
empirical formula	$C_{22}H_{21}FeN_3O$	$C_{11}H_{11}FeNO$
Fw	399.27	229.06
temp (K)	293(2)	293(2)
λ(Å)	0.71073	0.71073
cryst syst	Monoclinic	Monoclinic
space group	$P2_1/c$	$P2_1/c$
a (Å)	7.478(10)	10.4141(8)
b (Å)	17.45(2)	7.6611(6)
c (Å)	14.48(2)	12.1001(10)
β(°)	101.15(3)	95.271(3)
V (Å^3)	1854(4)	961.31(13)
Z	4	4
ρ_{calc} (Mg/m^3)	1.430	1.583
μ(Kα) (mm^{-1})	0.830	1.529
No. reflns.	36700	15009
Unique reflns.	3354	1765
GOOF (F^2)	1.10	1.101
R_{int}	0.078	0.0691
R1[a] ($I \geq 2\sigma$)	0.0375	0.0366
wR2[b] ($I \geq 2\sigma$)	0.0950	0.0617

[a] $R1 = \Sigma||F_o| - |F_c||/\Sigma|F_o|$. [b] $wR2 = [\Sigma[w(F_o^2 - F_c^2)^2]/ \Sigma[w(F_o^2)^2]]^{1/2}$.

3. Results and discussions

*3.1. Synthesis of ferrocene-based Schiff base **3** and ferrocenecarboxaldehyde oxime **4***

The reaction of ferrocenecarboxaldehyde **1** with 4-aminoantipyrine **2** in reluxing methanol furnishes the ferrocene-based Schiff base **3** in *ca.* 80% yield (Scheme 1).

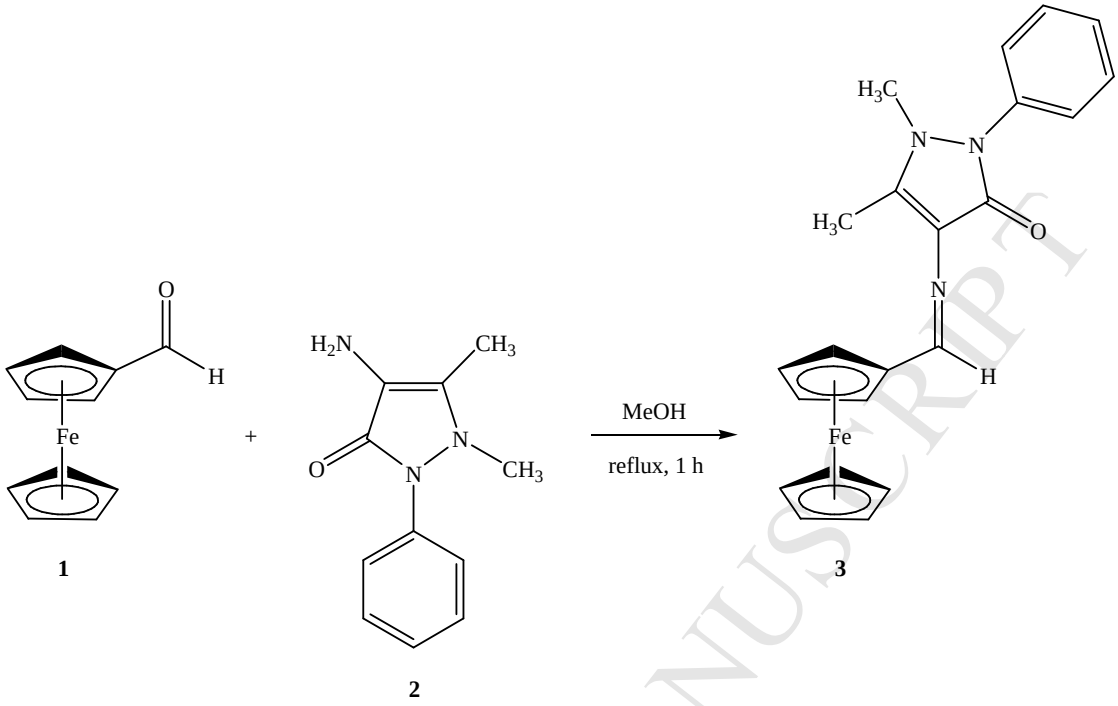

Scheme 1. Synthesis of ferrocene-based Schiff base **3** from ferrocenecarboxaldehyde **1** and 4-aminoantipyrine **2**.

Compound **3** was fully characterized by IR, ^{1}H and ^{13}C NMR spectroscopy, elemental analysis and also by single crystal X-ray diffraction (Fig. 2).

The IR spectrum of compound **3** does not show the typical carboxaldehyde C=O band at *ca.* 1750 cm^{-1} and displays a new strong band at 1642 cm^{-1} of the formed imine C=N group. In the ^{1}H NMR spectrum, the C*H*=N proton is detected at δ 9.52 ppm; the ^{13}C NMR resonances at δ 159.8 and 161.2 ppm confirm the presence of the amido (*C*(N)=O) and imino (*C*(H)=N) moieties, respectively.

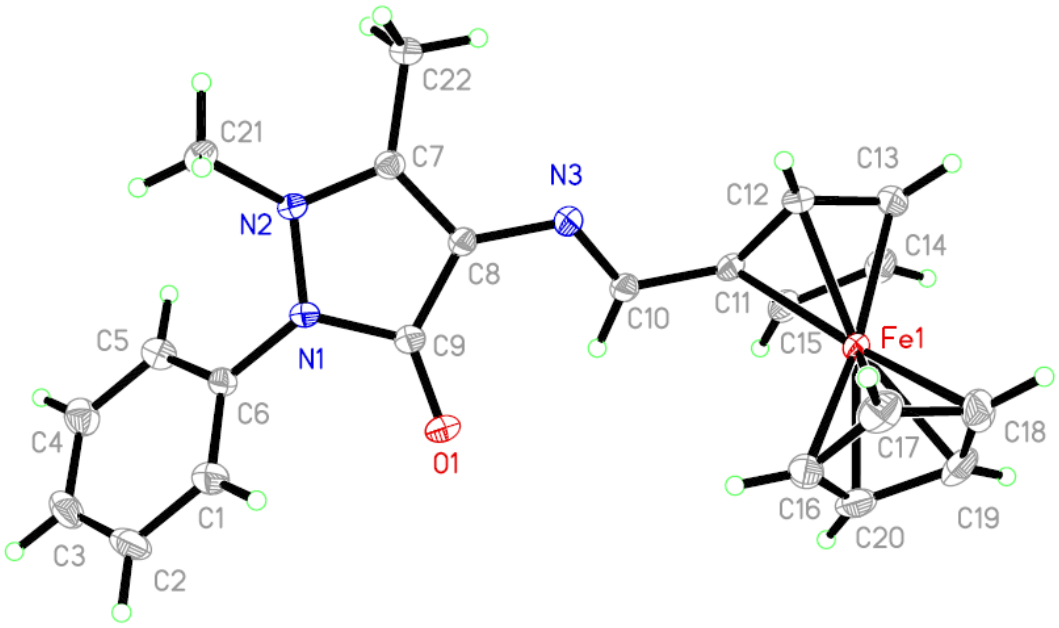

Fig. 2. Crystal structure of ferrocene-based Schiff base **3**.

On the other hand, the reaction of ferrocenecarboxaldehyde **1** with hydroxylamine in methanol, at room temperature, affords ferrocenecarboxaldehyde oxime **4** in *ca.* 85% yield (Scheme 2).

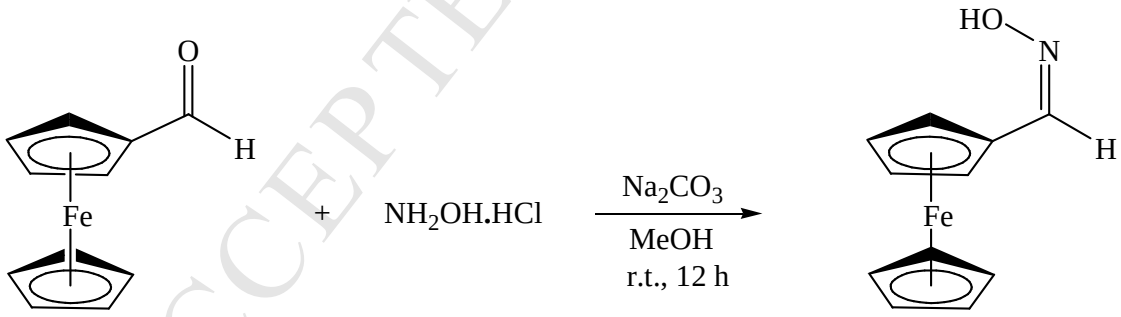

1 **4**

Scheme 2. Synthesis of ferrocenecarboxaldehyde oxime **4** from ferrocenecarboxaldehyde **1** and hydroxylamine hydrochloride.

Compound **4** was fully characterized by IR, ^{1}H, ^{13}C and DEPT-135 NMR spectroscopy, elemental analysis and also by single crystal X-ray diffraction (Fig. 3).

The IR spectrum of **4** does not show the typical C=O band at *ca.* 1750 cm^{-1} and displays new strong bands at 3195 and 1630 cm^{-1} due to hydroxyl (OH) and imine (C=N) groups, respectively. In the ^{1}H NMR spectrum, the C(*H*)=N proton is detected at δ 8.02 ppm. The ^{13}C NMR resonance at δ 150.0 ppm confirms the presence of the imino (*C*(H)=N) moiety. The DEPT-135 NMR shows the presence of the signal at δ 150.0 ppm which indicates that it concerns the tertiary carbon atom (*C*(H)=N).

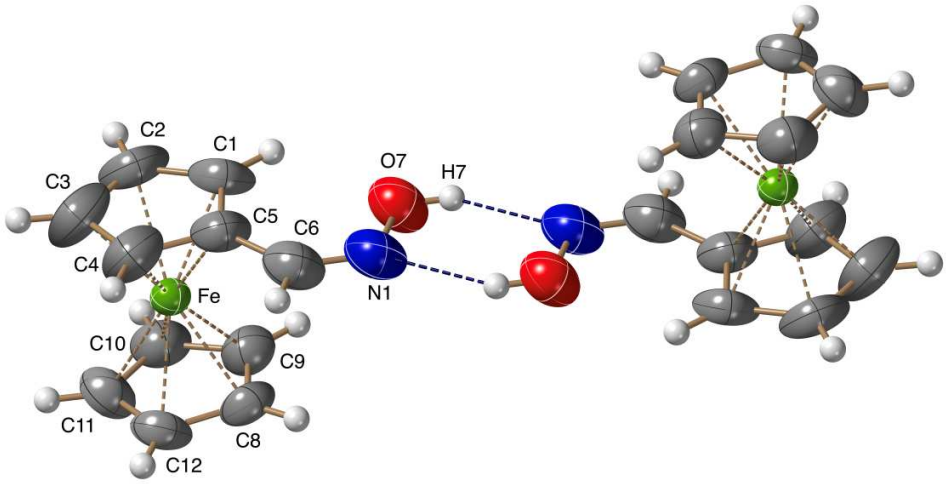

Fig. 3. The thermal ellipsoid plot of ferrocenecarboxaldehyde oxime **4** at 50% probability level. The neighboring molecules are linked together *via* disordered N-O-H groups (the second component, N1B-O7B-H7B, is omitted for clarity). Hydrogen bonds: O7-H7: 0.82 Å, H7···$N1^{\#}$: 2.09 Å, O7···$N1^{\#}$: 2.809(5) Å, O7-H7···$N1^{\#}$: 145.6°, O7B-H7B: 0.82 Å, H7B···$N1B^{\#}$: 2.04 Å, O7B···$N1B^{\#}$: 2.753 (12) Å, O7B-H7B···$N1B^{\#}$: 145.0°. Equivalent positions: # -x+1,-y+1,-z+2.

3.2. Effect of contact time

The effect of contact time on the adsorption of methyl blue dye (MB) by **3** and/or **4** is presented in Fig. 4. For both adsorbents, the amount of adsorbed MB was increased with an increase in time up to 40 min for **4** (82%) and 60 min in case of **3** (54%). When the contact time was up to 60 min and 120 min for **4** and **3**, respectively, the adsorption reaches equilibrium. It indicated that the short contact time is enough to adsorb 83% of

MB on **4** and 60% on **3**. Moreover, Fig. 4 shows that the adsorption capacity of **4** (0.129 mol g^{-1}) is higher than that of **3** (0.094 mol g^{-1}) towards MB. The maximum adsorption efficiency % of MB on various other adsorbents reported in the literature is shown in Table 2. The oxime species are known to undergo tautomerization to form nitrones [21]. Hence, the oxime Fc-C(H)=N-OH **4** (Fc = ferrocenyl) undergoes isomerization in aqueous solution to furnish the nitrone tautomer Fc-C(H)=$N^{(+)}$(H)-$O^{(-)}$ **4'**. This resulting cationic center in **4'** facilities the cation-anion interaction with anionic (MB) [22]. As a result, compound **4** shows higher adsorption capacity towards MB than **3**. However, the adsorption of MB on **3** is due to the π-π interaction between the benzene rings of MB and benzene ring in **3**. To illustrate the adsorption mechanism, the pseudo-first-order, the pseudo-second-order and intraparticle diffusion kinetic models were employed [23]. The equations of the three kinetic models are given in Eqs. (2), (3), and (4), respectively.

$$log(q_e - q_t) = log\ q_e - (k_1/2.303)\ t \quad (2)$$

$$t/q_t = 1/k_2 q_e^2 + t/q_e \quad (3)$$

$$q_t = k_p\ t^{1/2} + C \quad (4)$$

Where q_t, q_e are the adsorption capacity (mol g^{-1}) at time t and at equilibrium, respectively. k_1 is the pseudo-first-order equilibrium rate constant (min^{-1}), k_2 is the pseudo-second-order rate constant (mol g^{-1} min^{-1}). k_p represents the intraparticle diffusion rate constant (mol/g $min^{0.5}$) and C is a constant (mol g^{-1}) giving information about the boundary layer thickness. The slopes and the intercepts of each linear plot are used to calculate the kinetic parameters for MB adsorption. The results are listed in Table 3. Clearly, the pseudo-first-order model has high correlation coefficient ($R^2 \approx 0.996$ for **4** and $R^2 \approx 0.937$ for **3**) but the calculated equilibrium adsorbed capacity values (q_{ecal}) are far away from the experimental values (q_{eexp}), suggesting that this model don't fit the adsorption of MB onto both **3** and **4**. The correlation coefficients obtained from the pseudo-second-order model are higher than that of pseudo-first-order model and very closely to unity, indicating that the feasibility of pseudo-second-order kinetics model to describe the adsorption process of MB on both **3** and **4**. The good agreement between the

experimental data and pseudo-second-order can further be supported by the similar values of the experimental (q_{eexp}) and the calculated (q_{ecal}) from the kinetics equation.

For each adsorbent, the plot of q_t vs. $t^{1/2}$ yields two intersected straight segments, Fig. 5. The two intersected segments appeared in this confirm that adsorption takes place through two stages, a bulk diffusion followed by intraparticle diffusion [24]. The plot has zero intercept for **4** and away from passing through the origin in case of **3**, indicating that the intraparticle diffusion was the rate-controlling step for **4** and not sole rate-controlling step in **3**. So, the interactions of MB with the both **3** and **4** are best represented by a second order process with intraparticle diffusion, while liquid film diffusion is not playing any major role [25].

Table 2. Comparison of the maximum adsorption efficiency for the adsorption of MB onto various adsorbents reported in literature.

Adsorbent	Adsorption efficiency %	reference
Magnetic charcoal	64	[19]
Graphene oxide	58	[20]
Reduced graphene oxide	85	[20]
Compound **3**	60	This work
Compound **4**	83	This work

Table 3. Kinetics data with their correlation coefficient (R^2) for the adsorption of MB onto **3** and **4** at 20 °C.

Model	Parameters	Adsorbents	
		3	**4**
Pseudo-first order	q_e (10^{-2} mol g^{-1})	7.28	10.6
	k_1 (min^{-1})	0.037	0.076
	R^2	0.937	0.987
Pseudo-second order	$q_{e\ cal}$ (10^{-2} mol g^{-1})	9.94	13.6
	$q_{e\ exp}$ (10^{-2} mol g^{-1})	9.38	13.1
	k_2 (10^4 g mol^{-1} min^{-1})	1.05	0.213
	R^2	0.999	0.999
Intra-particle diffusion	k_{p1} (10^{-2} mol g^{-1} $min^{-0.5}$)	1.25	2.42
	R^2	0.969	0.991
	k_{p2} (10^{-3} mol g^{-1} $min^{-0.5}$)	2.90	1.22
	R^2	0.975	0.795

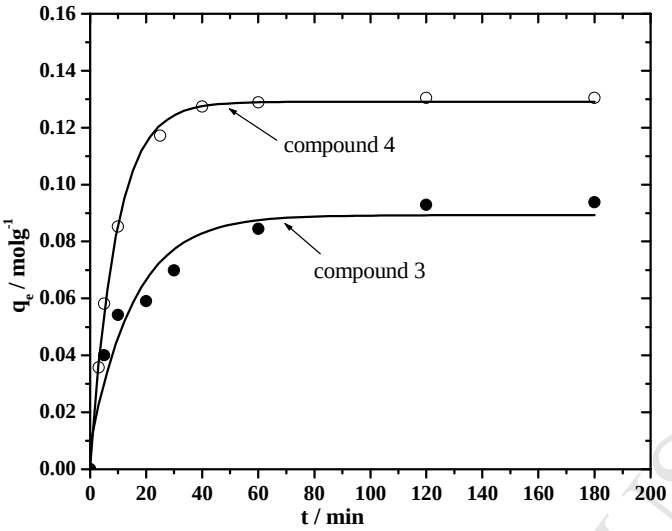

Fig. 4. Effect of contact time on the adsorption of MB on **3** and **4** (0.006 g) at 25°C and pH = 7. C_o = 2 x 10^{-4} M.

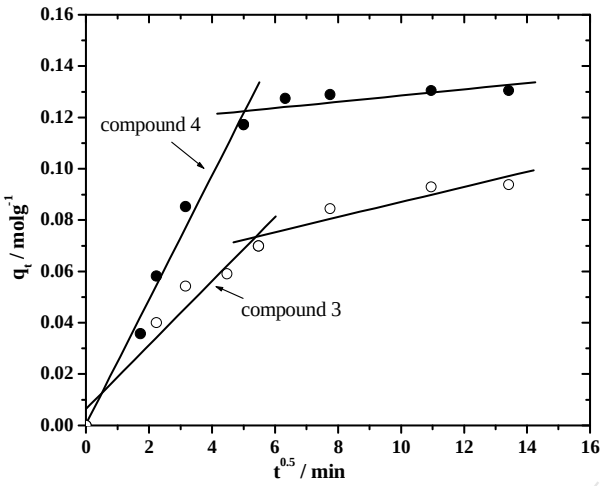

Fig. 5. Intraparticle diffusion plot for adsorption of MB onto **3** and **4** (0.006 g) at 25°C and pH = 7. C_o = 2 x 10^{-4} M.

3.3. Adsorption isotherm

The effect on the initial MB concentration on the adsorption capacity on by **3** and/or **4** was investigated and evaluated with the Freundlich and Langmuir isotherms. The calculated parameters of the Freundlich and Langmuir models associated with the correlation coefficient R^2 are presented in Table 4. Both models described similarly and quite well the experimental data. The maximum adsorption capacity (q_{max}) of **4** has higher than **3**. Also, the value of (q_{max}) of **4** was decreased with the increase of temperature while increased in case of **3**. This indicates that the adsorption was favorable at high temperature in case of **4** and at low temperature for **3**. The Freundlich constant (1/n) was less than unity for both adsorbents which implied that the adsorption of the MB onto **3** and/or **4** was favorable and also a possibility of multilayer adsorption onto the active heterogeneous adsorption sites of them [26]. Moreover, **4** has higher K_F than **3** reflecting the higher adsorption of **4** towards MB than **3** [22].

Table 4. Isotherm parameters and the correlation coefficient, R^2 for the adsorption of MB dye onto **3** and **4**.

Model	Parameters	Temperature (K)					
		293		303		313	
		3	**4**	**3**	**4**	**3**	**4**
Langmuir	q_{max} (mmol/g)	193	464	236	297	254	296
	K_L x 10^4 (L/mg)	23.3	4.29	20.6	6.16	16.8	7.52
	R^2	0.993	0.988	0.995	0.979	0.998	0.996
Freundlish	1/n	0.315	0.601	0.290	0.429	0.281	0.394
	K_F x 10^{-3} (mol/g)	4.61	143	2.54	16.7	3.96	12.3
	R^2	0.952	0.997	0.968	0.936	0.951	0.994

3.4. Thermodynamic parameters

Equilibrium data obtained at three different temperatures (20, 30 and 40 °C) were used to estimate the thermodynamic parameters of adsorption. Gibbs free energy change (ΔG^o), enthalpy change (ΔH^o), and entropy change (ΔS^o) for the adsorption of MB onto **3** and/or **4** were estimated using the following Eqs. (5), (6), and (7):

$$K_d = (q_e / C_e) \quad (5)$$

$$ln\ (K_d) = \Delta S^o/R - \Delta H^o/RT \quad (6)$$

$$\Delta G^o = \Delta H^o - T\,\Delta S^o \quad (7)$$

Where K_d is the distribution coefficient of the adsorbent, R (8.314 J mol^{-1} K^{-1}) is the universal gas constant, and T (K) is the absolute temperature of the solution. The values of ΔH^o and ΔS^o can be obtained from the slope and intercept of the van't Hoff plot (Eq. (6)), respectively. The determined values of ΔH^o, ΔS^o and ΔG^o are given in Table 5. The negative ΔH^o for MB-**4** system suggests that the adsorption is exothermic, while the

positive ΔH^o in case of MB-**3** indicates the endothermic nature of the adsorption and its low value indicates the adsorption to be physical in nature. The two adsorbents have negative ΔG^o means spontaneous adsorption in the temperature range studied [27]. Moreover, the negative value of ΔG^o decreased with increasing temperature, indicating that the spontaneous nature of adsorption of MB was proportional to the temperature [28]. However, positive ΔS^o is refers to the increasing of randomness at the solid/solution interface through the adsorption process. The decrease in ΔS^o value of **4** compared to that of **3** confirms the higher ability of **4** towards MB adsorption than **3** [22].

Table 5. Thermodynamic parameters of MB adsorbed onto **3** and **4**.

Adsorbent	Temp/K	K_d x 10^2/ Lg^{-1}	ΔH/ $kJmoL^{-1}$	ΔG/ $kJmoL^{-1}$	ΔS/ $JmoL^{-1}K^{-1}$
3	293	61.71	16.714	-21.26	129.6
	303	77.24		-22.55	
	313	77.80		-23.85	
4	293	109.2	-14.18	-22.53	28.53
	303	75.51		-22.82	
	313	95.67		-23.10	

4. Conclusions

Ferrocene-based Schiff base **3** and ferrocenecarboxaldehyde oxime **4** were synthetized, in very good yields, by reaction of ferrocenecarboxaldehyde **1** with 4-aminoantipyrine **2** or hydroxylamine, respectively. Compounds **3** and **4** were fully characterized by IR, ^1H, ^{13}C and DEPT-135 NMR spectroscopy, elemental analyses and also by single crystal X-ray diffraction. Both **3** and **4** are good adsorbents for MB from water. The adsorption capacity of **4** was higher than that of **3** due to the electrostatic interaction between cationic nitrogen center in **4** and the anionic MB. The adsorption kinetic was found to confirm pseudo-second-order. The adsorption behavior could be described by Langmuir and Freundlich isotherms. Furthermore, the adsorption process is spontaneous for both adsorbents and exothermic for **4** and endothermic in the case of **3**.

Appendix A. Supplementary data

CCDC 1812968 and 1812970 for **3** and **4**, respectively, contain the supplementary crystallographic data. These data can be obtained free of charge *via* http://dx.doi.org/....., or from the Cambridge Crystallographic Data Centre, 12 Union Road, Cambridge CB2 1EZ, UK; fax: (+44) 1223-336-033; or e-mail: deposit@ccdc.cam.ac.uk. Supplementary data associated with this article can be found, in the online version, at http://dx.doi.org/.....

References

[1] R.G. Saratale, G.D. Saratale, J.S. Chang, S.P. Govindwar, J. Taiwan Inst. Chem. Eng. 42 (2011) 138–157.

[2] Y. Wang, Y. Mu, Q. Zhao, H. Yu, Sep. Purif. Technol. 50 (2006) 1–7.

[3] L. Gan, S. Shang, E. Hu, C.W.M. Yuen, S.X. Jiang, Appl. Surf. Sci. 357 (2015) 866–872.

[4] Q. Wang, D. Zhang, S. Tian, P. Ning, J. Appl. Polym. Sci. 41029 (2014) 1–9.

[5] Y. Shao, X. Wang, Y. Kang, Y. Shu, Q. Sun, L. Li, J. Colloid Interface Sci. 429 (2014) 25–33.

[6] V.M. Daskalaki, E.S. Timotheatou, A. Katsaounis, D. Kalderis, Desalination 274 (2011) 200–205.

[7] S. Kaur, S. Rani, V. Kumar, R.K. Mahajan, M. Asif, I. Tyagi, V.K. Gupta, J. Ind. Eng. Chem. 26 (2015) 234–242.

[8] J. Lasri, M.F.C. Guedes da Silva, M.A. Januario Charmier, A.J.L. Pombeiro, Eur. J. Inorg. Chem. 23 (2008) 3668–3677.

[9] J. Lasri, M.A. Januario Charmier, M.F.C. Guedes da Silva, A.J.L. Pombeiro, Dalton Trans. (2007) 3259–3266.

[10] M.N. Kopylovich, V.Yu. Kukushkin, M.F.C. Guedes da Silva, M. Haukka, J.J.R. Fraústo da Silva, A.J.L. Pombeiro, J. Chem. Soc. Perkin Trans. 1, (2001) 1569–1573.

[11] M.N. Kopylovich, V.Yu. Kukushkin, M. Haukka, J.J.R. Fraústo da Silva, A.J.L. Pombeiro, Inorg. Chem. 41 (2002) 4798–4804.

[12] M.N. Kopylovich, V.Yu. Kukushkin, M. Haukka, K.V. Luzyanin, A.J.L. Pombeiro, J. Am. Chem. Soc. 126 (2004) 15040–15041.

[13] M.N. Kopylovich, J. Lasri, M.F.C. Guedes da Silva, A.J.L. Pombeiro, Dalton Trans. (2009) 3074–3084.

[14] H.-F. Wu, H.-X. Wang, Acta Cryst. E61 (2005) m580–m581.

[15] S.C.B. Gnoatto, A. Dassonville-Klimpt, S. Da Nascimento, P. Galéra, K. Boumediene, G. Gosmann, P. Sonnet, S. Moslemi, Eur. J. Med. Chem. 43 (2008) 1865–1877.

[16] Bruker AXS, APEX3 – Software Suite for Crystallographic Programs (2016). Bruker AXS, Inc.: Madison, WI, USA.

[17] G.M. Sheldrick, (2016). SADABS - Bruker Nonius scaling and absorption correction, Bruker AXS, Inc.: Madison, Wisconsin, USA, 2.

[18] G.M. Sheldrick, Acta Cryst. C71 (2015) 3–8.

[19] P. Sharma, D.J. Borah, P. Das, M.R. Das, Desalin. Water Treat. 57 (2016) 8372–8388.

[20] A. Sari, D. Mendil, M. Tuzen, M. Soylak, J. Hazard. Mater. 162 (2009) 874–879.

[21] D. Roca-López, A. Darù, T. Tejero, P. Merino, RSC Adv., 6 (2016) 22161–22173.

[22] A.S. Elsherbiny, M.E. El-Hefnawy, A.H. Gemeay, Chem. Eng. J. 315 (2017) 142–151.

[23] S. Dadfarnia, A.M. Haji Shabani, S.E. Moradi, S. Emami, Appl. Surf. Sci. 330 (2015) 85–93.

[24] L. Jiang, Y. Liu, S. Liu, X. Hu, G. Zeng, X. Hu, S. Liu, S. Liu, B. Huang, M. Li, Chem. Eng. J. 308 (2017) 597–605.

[25] J. Chang, J. Ma, Q. Ma, D. Zhang, N. Qiao, M. Hu, H. Ma, Appl. Clay Sci. 119 (2016) 132–140.

[26] A. Vanaamudan, P.P. Sudhakar, J. Taiwan Inst. Chem. Eng. 55 (2015) 145–151.

[27] H. Liu, X. Ren, L. Chen, J. Ind. Eng. Chem. 34 (2016) 278–285.

[28] Y. Shao, L. Zhou, C. Bao, J. Ma, M. Liu, F. Wang, Chem. Eng. J. 283 (2016) 1127–1136.

HIGHLIGHTS

* Ferrocene-based Schiff and ferrocenecarboxaldehyde oxime were synthetized and fully characterized.

* Adsorption efficiency of both compounds toward methyl blue dye was examined.

* Kinetics and thermodynamic parameters of the adsorption process were studied.